Acetaldehyde on Pt(111) and Pt/Sn(111): A DFT Study of the Adsorption Structures and of the Vibrational Spectra

Françoise Delbecq* and Fabienne Vigné

Laboratoire de Chimie, UMR CNRS 5182, Ecole Normale Supérieure de Lyon, 46 allée d'Italie, 69364 Lyon Cedex 07, France

Received: October 20, 2004; In Final Form: April 7, 2005

The relative stability of the $\eta_1\mu_1$ (atop) and $\eta_2\mu_2$ (di-σ) geometries of acetaldehyde are compared on Pt(111) and on two PtSn alloys ((2×2) and $(\sqrt{3} \times \sqrt{3})R30°$) by means of density functional theory (DFT) calculations. At low coverage on Pt ($^1/_9$ ML), the two forms are equivalent in energy, with $\eta_1\mu_1$ being slightly more stable. At high coverage ($^1/_4$ and $^1/_3$ ML), $\eta_2\mu_2$ is less competitive and acetaldehyde is adsorbed through the aldehydic hydrogen. The evolution of the adsorption energy with the coverage and the apparition of the structure adsorbed through the aldehydic hydrogen are explained by the existence of attractive dipole−dipole interactions. On PtSn, only the $\eta_1\mu_1$ geometry is stable with an adsorption energy equal to that on Pt, in agreement with temperature-programmed desorption (TPD) experiments. The calculated vibrational spectra allow us to conclude that the experimental spectrum corresponds to a mixture of $\eta_1\mu_1$ (majority) and $\eta_2\mu_2$ (minority) structures on Pt and to only $\eta_1\mu_1$ on PtSn. The various interactions and the relative stability of the species on Pt and PtSn are explained by the density of states (DOS) curves.

Introduction

Reactions of aldehydes on transition metal surfaces are important in catalysis for many processes. For example, aldehydes are obtained during the production of hydrogen from alcohols in fuel cells, particularly acetaldehyde from ethanol. Another application is the selective hydrogenation of $\alpha-\beta$ unsaturated aldehydes to produce unsaturated alcohols. Pt and Pt alloy catalysts have been widely tested to improve the selectivity. The Pt/Sn surface alloys have been found to be very efficient.[1] Hence, it is of interest to understand aldehyde adsorption on Pt and Pt/Sn alloys.

The adsorption of aldehydes on surfaces is far less studied than that of alkenes, as well experimentally as theoretically. For acetaldehyde on Pt particularly, a few experimental studies exist: an old one on a stepped Pt surface,[2] one on Pt(111),[3] and a recent one on Pt(111) and on the surface alloys Pt/Sn-(111).[4] In the latter, it is concluded that acetaldehyde is adsorbed in an $\eta_1\mu_1$ (atop) geometry on Pt and on the alloys, with similar adsorption energies. These conclusions are based on temperature-programmed desorption (TPD) experiments and high-resolution electron energy loss spectroscopy (HREELS) spectra. A few theoretical studies deal with the adsorption of acetaldehyde on Pt(111);[5−7] however, the results are contradictory concerning the adsorption geometry and the adsorption energy. In refs 5 and 6, acetaldehyde is considered as $\eta_2\mu_2$ (di-σ) bounded and in ref 7 as $\eta_1\mu_1$ (atop through the oxygen atom). In the case of adsorption on Pt/Sn alloys, no theoretical study exists for acetaldehyde. However, the adsorption of unsaturated aldehydes on Pt(111) and Pt/Sn(111) has been studied recently.[8,9] In tight connection with this study, we were interested in the comparison of the acetaldehyde behavior on these metal surfaces.

Hence, in the present paper, we will first compare the two possible adsorption geometries of acetaldehyde on Pt(111) and Pt/Sn(111) by means of calculations based on the density functional theory (DFT). Then, we will simulate the vibrational spectra of these structures and try to attribute the experimental spectra to one of them, to confirm the nature of the adsorbed species. We will finally examine the acetaldehyde interactions with the surface in terms of density of states (DOS) analysis.

Computational Details

The calculations were performed with the Vienna ab initio simulation package (VASP).[10−12] This program performs periodic density functional theory calculations using a plane-wave basis set. The calculations were done at the generalized gradient approximation (GGA) level with the functional of Perdew and Wang 91.[13] We used the frozen core projector-augmented-wave (PAW) method.[14]

The surfaces were modeled by periodic four-layer slabs, with adsorption on one side of the slab. Experimentally, the surface alloys are obtained by Sn vapor deposition followed by annealing. Depending on the amount of Sn, two structures are formed, namely, (2×2) with stoichiometry Pt_3Sn and $(\sqrt{3} \times \sqrt{3})R30°$ with stoichiometry Pt_2Sn.[15] XPD data have shown that these alloys are two-dimensional surface alloys.[16] Hence, in the model chosen for the surface alloys, only the first layer contains Sn atoms in the two stoichiometries given just above. Each slab is separated from its periodic image in the *z* direction by a vacuum space corresponding to five layers (11.5 Å). One molecule is adsorbed per unit cell. For the adsorption on Pt-(111), four different unit cells were used. They contain nine, six, four, and three atoms per layer, respectively, giving 3×3, 2×3, 2×2, and $\sqrt{3} \times \sqrt{3}$ adsorption structures and coverages of $^1/_9$, $^1/_6$, $^1/_4$, and $^1/_3$ ML. The Brillouin zone integration has been done on a $3 \times 3 \times 1$ grid for a coverage of $^1/_9$ ML, on a $5 \times 3 \times 1$ grid for a coverage of $^1/_6$ ML, and on a $5 \times 5 \times 1$ grid for coverages of $^1/_4$ and $^1/_3$ ML. For the (2×2) Pt_3Sn alloy, only one unit cell corresponding to a low coverage was considered: it contained eight atoms per layer, which gives a 4

* Corresponding author. E-mail: francoise.delbecq@ens-lyon.fr.

10.1021/jp045207j CCC: $30.25
Published on Web 05/05/2005

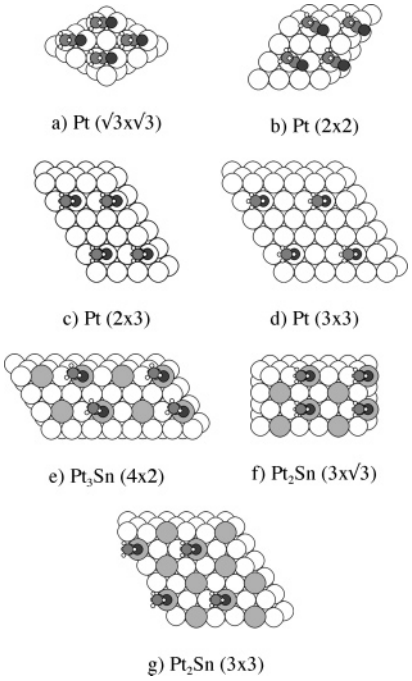

Figure 1. Representation of the Pt(111) surface used for the chemisorption at coverages of $^1/_3$, $^1/_4$, $^1/_6$, and $^1/_9$ ML, of the surface of the alloy p(2 × 2) $Pt_3Sn(111)$ at a coverage of $^1/_8$ ML, and of the alloy $(\sqrt{3} \times \sqrt{3})R30°$ $Pt_2Sn(111)$ at coverages of $^1/_6$ and $^1/_9$ ML. An example of the $\eta_1\mu_1$(O) adsorption of acetaldehyde is shown (Pt, large white; Sn, large gray; C, medium gray; O, medium black; H, small white). The periodicity of the molecules indicates the unit cell: (a) $\sqrt{3} \times \sqrt{3}$; (b) 2 × 2; (c) 2 × 3; (d) 3 × 3; (e) 4 × 2; (f) 3 × $\sqrt{3}$; (g) 3 × 3.

× 2 adsorption structure and a coverage of $^1/_8$ ML. The Brillouin zone integration has been done on a Γ centered 2 × 4 × 1 grid. For the $(\sqrt{3} \times \sqrt{3})R30°$ Pt_2Sn alloy, a coverage of $^1/_6$ ML (with a 3 × 5 × 1 grid), which gives a 3 × $\sqrt{3}$ adsorption structure, and a coverage of $^1/_9$ ML as on Pt(111) were studied. All these systems are depicted in Figure 1.

For the frozen part of the slab, the same metal interatomic distance (2.82 Å) was used in the case of pure platinum and in the case of the alloys (optimized from Pt bulk calculations). This is justified by the fact that experimentally the lattice parameter is imposed by the underlying Pt bulk and the Sn atoms in the uppermost layer accommodate this constraint by an outward displacement.[15] For all structures, the geometry optimization included all degrees of freedom of the adsorbed molecule and of the two uppermost metal layers. The gas phase molecule was also calculated periodically in a large cubic box (20 × 20 × 20 $Å^3$). The adsorption energy is defined as the difference between the energy of the whole system and the sum of the energies of the bare slab and of the gas phase adsorbate. A negative value means a stabilizing adsorption.

Since the molecules are adsorbed on only one side of the slab, the unit cell has a net dipole and a spurious electrostatic interaction between the slab and its periodic images can modify the total energy. A correction has been applied both on the energy and on the potential, to remove this effect. This correction does not exceed 40 meV for Pt and 70 meV for the alloys. The energy values given hereafter are the corrected ones.

The HREELS spectra were simulated by calculation of the vibrational frequencies.[17] The technique for calculating these frequencies is based on the numerical calculation of the second derivatives of the potential energy surface within the harmonic approach. The coupling with the surface phonons is neglected. Indeed, we have verified that the interesting frequencies (above 400 cm^{-1}) are not affected by this coupling. The force constant matrix is built with finite differences of the first derivatives of the total energy by geometrical perturbations of the optimized Cartesian coordinates of the system. The diagonalization of this matrix provides the harmonic molecular frequencies and the associated harmonic normal vibration modes. The intensities of the EELS spectra are estimated by applying the formula given in ref 18 where the intensities are proportional to the square of the dynamic dipole moments (derivatives of the dipole moments with respect to a given normal mode), to a function depending on experimental parameters and to the inverse of the frequencies. In the specular mode used for the HREELS spectra, the main contribution to the intensity is the component of the dynamic dipole moments normal to the surface.

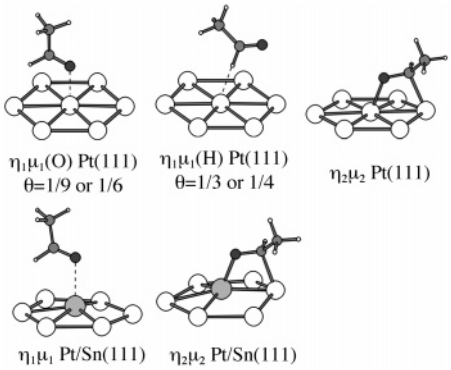

Figure 2. Various adsorption geometries ($\eta_1\mu_1$ and $\eta_2\mu_2$) of acetaldehyde on Pt(111) and on the Pt/Sn alloys. In the case of adsorption on Pt at $^1/_3$ and $^1/_4$ ML, the interaction takes place through the H atom ($\eta_1\mu_1$(H)).

TABLE 1: Main Bond Lengths (in Å) in the Various Adsorption Geometries of Acetaldehyde on Pt(111), (2 × 2) $Pt_3Sn(111)$, and $(\sqrt{3} \times \sqrt{3})$ $Pt_2Sn(111)$ at Various Coverages (θ)

	site	θ	M−O[a]	M−C[a]	C−O[b]	C−C[b]	Pt−H_{ald}[b]	C−H_{ald}
Pt	$\eta_1\mu_1$(O)	$^1/_9$	2.31		1.23	1.49	2.63	1.12
		$^1/_6$	2.50		1.23	1.49	2.55	1.12
	$\eta_1\mu_1$(H)	$^1/_4$	3.92		1.22	1.49	2.31	1.15
		$^1/_3$	3.52		1.22	1.49	2.38	1.14
	$\eta_2\mu_2$	$^1/_9$	2.08	2.19	1.34	1.51	2.53	1.11
		$^1/_6$	2.09	2.17	1.35	1.51	2.53	1.11
		$^1/_4$	2.09	2.17	1.35	1.51	2.52	1.11
		$^1/_3$	2.10	2.19	1.34	1.51	2.53	1.11
Pt_3Sn	$\eta_1\mu_1$/Pt[c]	$^1/_8$	3.17		1.22	1.50	3.12	1.12
	$\eta_1\mu_1$/Sn[c]	$^1/_8$	2.67		1.23	1.49	2.68	1.12
	$\eta_2\mu_2$/Sn[c]	$^1/_8$	2.16	2.24	1.34	1.51	2.52	1.11
Pt_2Sn	$\eta_1\mu_1$/Sn[c]	$^1/_9$	2.58		1.23	1.49	2.87	1.12
		$^1/_6$	2.69		1.23	1.50	3.01	1.12
	$\eta_2\mu_2$/Sn[c]	$^1/_9$	2.14	2.23	1.35	1.51	2.55	1.11

[a] M = Pt or Sn. [b] For comparison, in the gas phase: C=O, 1.22 Å; C−C, 1.50 Å; C−H, 1.12 Å. [c] $\eta_1\mu_1$/Pt, atop Pt; $\eta_1\mu_1$/Sn, atop Sn; $\eta_2\mu_2$/Sn, C interacts with Pt and O with Sn.

Results and Discussion

Adsorption. The various optimized adsorption geometries atop ($\eta_1\mu_1$) and di-σ ($\eta_2\mu_2$) on Pt(111) and on the two alloys are shown in Figure 2 for different coverages. The corresponding bond lengths are given in Table 1. For the atop geometry, the optimization gives different structures depending on the coverage. On Pt(111) at $^1/_9$ and $^1/_6$ ML, acetaldehyde is bound to the surface through the oxygen atom with a Pt−O distance of 2.31 and 2.50 Å, respectively, and a C−O distance of 1.23 Å in agreement with previous calculations on aldehydes.[7,8] This structure will be called hereafter $\eta_1\mu_1$(O). For $^1/_4$ and $^1/_3$ ML, the oxygen atom goes away from the surface during the

TABLE 2: Adsorption Energies (in kJ/mol) of Acetaldehyde on Pt(111), (2 × 2) Pt_3Sn(111), and ($\sqrt{3} \times \sqrt{3}$) Pt_2Sn(111) at Various Coverages (θ)

	Pt				Pt_3Sn	Pt_2Sn	
θ	1/3	1/4	1/6	1/9	1/8	1/6	1/9
$\eta_1\mu_1$	−27[a]	−28[a]	−19[b]	−27[b]	−29[c]	−19[c]	−27[c]
$\eta_2\mu_2$	−17	−25	−24	−23	−2[c]		−1[c]

[a] $\eta_1\mu_1$(H): adsorbed by the aldehydic hydrogen. [b] $\eta_1\mu_1$(O): adsorbed by the oxygen atom. [c] The oxygen atom is adsorbed on Sn.

optimization and the molecule rotates so that an interaction occurs between the aldehydic hydrogen and a Pt atom. The resulting structure will be called $\eta_1\mu_1$(H). This process is the most pronounced in the case of 1/4 ML: the Pt−O distance becomes 3.92 and 3.52 Å and the Pt−H distance becomes 2.31 and 2.38 Å for 1/4 and 1/3 ML, respectively. The Pt−H interaction is accompanied by a lengthening of the C−H bond from 1.12 to 1.15 and 1.14 Å. Therefore, when the coverage increases, the atop geometry evolves into a structure bound by the aldehydic hydrogen. As shown in Table 2, this structure is stable, since the corresponding binding energy is similar to the one obtained for $\eta_1\mu_1$(O) at 1/9 and 1/6 ML: −27 and −28 kJ/mol at 1/3 and 1/4 ML, respectively.

On the Pt/Sn alloys, two atop sites can exist, one above a Pt atom and one above a Sn atom. The $\eta_1\mu_1$/Pt structure is less stable on Pt_3Sn than on platinum (adsorption energy of −8 kJ/mol). In fact, the Pt−O distance is long (3.17 Å, see Table 1) and acetaldehyde is rather physisorbed. On Pt_2Sn, it does not exist. In contrast, the $\eta_1\mu_1$/Sn structure is stable on both alloy surfaces with a binding energy equal to the one found on platinum: −29 and −27 kJ/mol for Pt_3Sn at 1/8 ML and Pt_2Sn at 1/9 ML, respectively, and −19 kJ/mol for Pt_2Sn at 1/6 ML. The Sn−O lengths are rather long: 2.67 Å for (2 × 2) Pt_3Sn and 2.58 and 2.69 Å for ($\sqrt{3} \times \sqrt{3}$) Pt_2Sn at coverages of 1/9 and 1/6 ML, respectively. As in the case of Pt(111), one observes a lengthening of the metal−oxygen bond when the coverage increases, which can be related to stronger interactions between the adsorbed molecules. The other bonds are similar to those calculated for the atop site $\eta_1\mu_1$(0) on platinum.

The di-σ adsorbed structure does not vary much with the coverage. The Pt−O and Pt−C bond lengths given in Table 1 are close to those found in previous works.[5,8] The C−O bond lengthens upon adsorption from 1.22 to 1.34 or 1.35 Å, as also found previously. The adsorption energy varies weakly with the coverage between −17 and −25 kJ/mol.

In the case of the alloys, there are two possibilities for the di-σ adsorption: either C and O interact with a Pt atom or C interacts with a Pt atom and O with a Sn atom, the opposite situation being excluded.[9] The adsorption on two Pt atoms is not stable whatever the alloy, as it has been already noticed for other aldehydes.[9] The adsorption on a Pt and a Sn atom was calculated to be stable but with a very low binding energy (2 and 1 kJ/mol for Pt_3Sn and Pt_2Sn, respectively) at the limit of the method accuracy. The geometries are not different from those found on platinum except for a slightly longer Pt−C bond.

The foregoing results show that two adsorbed structures can exist with close adsorption energies whatever the coverage (Table 2). At low coverage (1/9 ML), these structures are the $\eta_2\mu_2$ and $\eta_1\mu_1$(O) ones, the latter being more stable by only 4 kJ/mol. At medium coverage (1/6 ML), the adsorption energy of the $\eta_1\mu_1$(O) geometry is decreased (from −27 to −19 kJ/mol) but that of the $\eta_2\mu_2$ geometry is slightly increased (from −23 to −24 kJ/mol) so that the latter geometry becomes the most stable. Our adsorption energies are slightly different from those found by others for the same coverages,[5,7] which is probably due to the smaller thickness of the slabs they used. At higher coverage (1/4 and 1/3 ML), the $\eta_2\mu_2$ geometry still exists, while the atop one transforms into $\eta_1\mu_1$(H). At 1/4 ML, the two geometries have similar adsorption energies (−25 and −28 kJ/mol), while, at 1/3 ML, $\eta_1\mu_1$(H) is the most stable one. Such a structure seems to be usual for aldehydes on Pt(111), since we have found a similar one during the desorption of propanal from the atop geometry.[19]

SCHEME 1: Dipole−Dipole Interactions in the Various Adsorption Geometries of Acetaldehyde

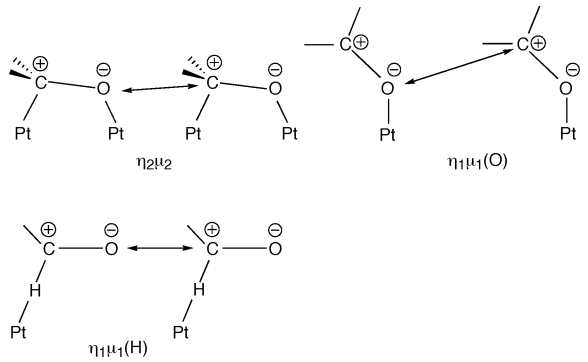

TABLE 3: Stabilizing Contribution of the Dipole−Dipole Interactions (in eV) to the Energy of a Film of Gas Phase Acetaldehyde Molecules in the Adsorbed Geometries at Different Coverages on Pt(111) (*a* and *b* Are the Directions of the Lattice Vectors in the Surface Plane)

θ		1/3	1/4	1/6	1/9
$\eta_1\mu_1$(O)	*a*		0.16[a]	0.09	0.02
	b		0.0	0.0	0.0
$\eta_1\mu_1$(H)	*a*	0.23	0.36		
	b	0.26	0.06		
$\eta_2\mu_2$	*a*	0.24	0.29	0.14	0.03
	b	0.29	0.0	0.0	0.0

[a] The geometry used is the one obtained for a coverage of 1/6 ML, since, at 1/4 ML, the $\eta_1\mu_1$(O) structure does not exist as a stable species.

One notices that the adsorption energy of the $\eta_2\mu_2$ geometry on Pt(111) increases up to a coverage of 1/4 ML but decreases for a coverage of 1/3 ML. Conversely, the adsorption energy of the $\eta_1\mu_1$(O) geometry decreases from 1/9 to 1/6 ML (as it does also on Pt_2Sn) and then that of the $\eta_1\mu_1$(H) geometry is again larger. Usually, due to steric hindrance, the adsorption energy decreases when the coverage increases. In the present case, the variation of the adsorption energy with the coverage can be explained if dipole−dipole interactions are taken into account. Due to the C═O bond, acetaldehyde is a polar molecule. For the $\eta_2\mu_2$ geometry, the C═O bonds are almost parallel to the surface (Figure 2) and the attractive interactions are maximum (see Scheme 1). For the $\eta_1\mu_1$(O) geometry, the C═O bonds are inclined relative to the surface and their interactions are smaller. Finally, for the $\eta_1\mu_1$(H) geometry, the C═O bonds are again parallel to the surface, even more than for the $\eta_2\mu_2$ geometry. The dipole−dipole interactions have been quantified in the direction of the lattice vectors *a* and *b* as follows: films of gas phase acetaldehyde molecules have been considered in the adsorbed geometries for the various coverages. Removal of the dipole interactions in directions *a* and *b* allows us to obtain the resulting destabilization. The results are given in Table 3. For a small coverage (1/9 ML), the interactions are quasi-nonexistent. When the coverage increases, they become larger but more for $\eta_2\mu_2$ than for $\eta_1\mu_1$(O). In the former case, they overbalance the steric effects up to a coverage of 1/4 ML. At a coverage of 1/3 ML, the steric interactions become dominant, which leads to a decrease of the adsorption energy. For the $\eta_1\mu_1$(H) geometry,

at a high coverage of $^1/_4$ or $^1/_3$ ML, the dipole−dipole interactions are very important, which explains the large adsorption energies obtained for this structure. The existence of these strong stabilizing dipole−dipole interactions explains the evolution of $\eta_1\mu_1$(O) to $\eta_1\mu_1$(H) at high coverage. The same behavior has already been found for other aldehydes but has not been analyzed as much.[8] The monolayer acetaldehyde coverage has been estimated experimentally to correspond to 0.35 ML, hence, close to a coverage of $^1/_3$ ML.[4] That means that the monolayer would be constituted by $\eta_1\mu_1$(H) molecules. However, it is obvious that these dipole interactions exist if the molecules are adsorbed periodically with the same orientation. If their orientation is more random, these interactions can cancel each other. In such a case, the $\eta_1\mu_1$(O) geometry can remain stable and then does not evolve to $\eta_1\mu_1$(H).

On the alloys Pt_3Sn and Pt_2Sn, the situation is more simple, since only the $\eta_1\mu_1$(O) structure, with O bound to a Sn atom, is stable (Table 2). Neither $\eta_2\mu_2$ nor $\eta_1\mu_1$/Pt is stable. The adsorption energies are very close to that obtained on Pt(111) for the same coverage ($^1/_9$ ML). This is in agreement with the experimental TPD results.[4] Effectively, the desorption temperature is 148 K on platinum and 158 K on the alloys, which shows that the binding energy is similar on the pure metal and on its alloys. From these temperatures, the desorption activation energies were estimated to be 37 and 40 kJ/mol, respectively. These values represent an upper limit for the adsorption energies, as verified from our values.

Vibrational Spectra. One way to characterize the species adsorbed on a surface is to perform their vibrational spectra. The precise optimization of the adsorbed structures allowed us to calculate the vibrational frequencies in order to simulate the HREELS spectra. To validate the computational method, we have calculated first the vibrational spectrum of acetaldehyde in the gas phase. This spectrum has given rise to numerous experimental studies because the analysis was complicated by the occurrence of Coriolis and Fermi resonances.[20] All the modes have been finally assigned,[21,22] and it results that the gas phase corrected spectrum and the crystalline phase spectrum are very similar, since the Coriolis and Fermi resonances are lifted in the crystal spectra. Obviously, the calculations can only give the fundamentals and not the resonances. The optimization of the gas phase molecule gives bond lengths in good agreement with the experimental values: 1.22 Å for C═O, 1.50 Å for C−C, and 1.12 Å for C−H_{ald}.[20] The calculated frequencies of the 15 fundamentals and their mode assignments are given in Table 4 together with the experimental values from ref 20. The CH stretches ($\nu_1-\nu_3$ and ν_{11}) are not well described in terms of energy, as is often the case, which is partly due to their anharmonicity, not taken into account in the present calculations. For the other modes, there is good agreement of our values with the experimental ones if we keep in mind that no scaling factor is applied. Our assignments also confirm those given experimentally.

The frequencies obtained for the atop and di-σ geometries of acetaldehyde on Pt(111) at various coverages are given in Table 5 with the mode assignments. The calculated spectra taking the peak intensities into account are shown in Figure 3. The spectra for the $\eta_1\mu_1$(O) geometry at $^1/_6$ and $^1/_9$ ML (Figure 3c and e) show a great similarity. The modes and the frequencies are similar to those obtained for the gas phase (compare with Table 4) except for the νCO stretch that is pushed toward lower frequencies by the interaction with the surface. The spectra are characterized by high peaks at 1682−1635, 1100−1096, 884−882, and 503−509 cm^{-1}, corresponding to νCO, νCC, ρCH_3, and νPtO, respectively, and by several medium peaks between 1319 and 1357 cm^{-1} and between 1317 and 1394 cm^{-1}, corresponding to δ modes. As before, the CH stretches (around 3000 cm^{-1}) are not well described in terms of energy and also of intensity. For example, the intensity has to be multiplied by 10 in order to have a significant height in the calculated spectra, whereas they give a large and intense peak in the experimental spectrum that is reproduced in Figure 4 (from ref 4). The same observation has been done in the case of acrolein.[17] The small intensity of the νCH stretches seems to be due to the presence of the large C═O permanent dipole.

TABLE 4: Experimental and Calculated Vibrational Frequencies (in cm^{-1}) of Acetaldehyde in the Gas and Crystalline Phases

assignment	description[a]	gas phase[21]	crystalline phase[21]	calculated gas phase (this work)
ν_1 (a′)	ν_aCH_3	3014	3003	3087
ν_{11} (a″)	ν_aCH_3	2966	2964	3020
ν_2 (a′)	ν_sCH_3	2923	2918	2967
ν_3 (a′)	νCH_{ald}	2750[b]	2747	2790
ν_4 (a′)	νCO	1743	1722	1755
ν_{12} (a″)	δ_aCH_3	1436[c]	1431	1422
ν_5 (a′)	δ_aCH_3	1430[c]	1422	1411
ν_6 (a′)	δCCH_{ald}	1395	1389	1374
ν_7 (a′)	νCC, δ_sCH_3	1352	1347	1324
ν_8 (a′)	ρ_sCH_3, νCC	1114[c]	1118	1096
ν_{13} (a″)	γCH_{ald}, ρ_aCH_3	1107[c]	1102	1089
ν_9 (a′)	νCC, ρ_sCH_3	875[b]	882	870
ν_{14} (a″)	ρ_aCH_3, γCH_{ald}	764	770	747
ν_{10} (a′)	δCCO	509	519	491
ν_{15} (a″)	τCH_3	143[d]		164

[a] Symmetry a′: ν_aCH_3 (asym methyl CH stretch), ν_sCH_3 (sym methyl CH stretch), νCH_{ald} (carbonyl CH stretch), νCO (CO stretch), νCC (CC stretch), δ_aCH_3 (asym CH_3 deformation), δ_sCH_3 (sym CH_3 deformation), δCCH_{ald} (in-plane CH wag), ρ_sCH_3 (in-plane CH_3 rock), δCCO (CCO bend). Symmetry a″: ν_aCH_3 (methyl CH stretch), δ_aCH_3 (CH_3 deformation), ρ_aCH_3 (out-of-plane CH_3 rock), γCH (out-of-plane CH wag), τCH_3 (torsion). [b] Values corrected for Fermi resonance. [c] Coriolis resonance bands between ν_5 and ν_{12} and ν_8 and ν_{13}, respectively.[21] [d] Reference 22.

The spectrum for the H-bound structure at $^1/_3$ ML ($\eta_1\mu_1$(H), Figure 3a) is different: it presents a very weak νCO stretch and, on the contrary, an intense and low νCH_{ald} stretch at 2578 cm^{-1}. The latter peak is due to the interaction of the aldehydic H with the surface and the concomitant lengthening of the C−H bond. Such a low νCH frequency exists also in the spectra of adsorbed alkanes: 2590 cm^{-1} for cyclohexane on Pt(111)[23] or 2605 cm^{-1} in the case of norbornadiene.[24] The other peaks appear at 1348, 1107, 887, and 509 cm^{-1} and correspond to δCCH, two (νCC, ρCH_3) and (νPtH, δCCO) modes, respectively. The same spectrum is obtained for a coverage of $^1/_4$ ML (not shown), with an even lower νCH_{ald} stretch at 2431 cm^{-1}, owing to the shorter Pt−H bond and the longer C−H bond.

The spectra for the di-σ geometry are characterized by high peaks at [1048, 1000 and 980], [827, 807 and 793], [546, 540 and 534], [427, 430 and 423] cm^{-1} and smaller peaks at 1294 and 1295 cm^{-1} for coverages of $^1/_3$, $^1/_6$, and $^1/_9$ ML, respectively (Figure 3b, d, and f). These peaks correspond to (ρCH_3, νPtC), (νCO, γCH_{ald}), (νPtC, νPtO), (νPtC, ρCH_3), and (νCC, δCCH, δCH_3), respectively. The νCO stretch is visible, although the C═O bond is parallel to the surface, because it is coupled with the wagging of the aldehydic H (γCH_{ald}). One can notice from Figure 3 that the more intense peaks for the $\eta_1\mu_1$(H), $\eta_1\mu_1$(O), and $\eta_2\mu_2$ forms are at different frequencies without almost any overlap, which will help us to identify these geometries by comparison with the experimental spectra.

Undoubtedly, the absence in the experimental spectrum of a low νCH peak around 2400−2600 cm^{-1} excludes the existence

TABLE 5: Vibrational Frequencies (in cm^{-1}) of the Adsorption Geometries of Acetaldehyde on Pt(111) at Various Coverages (θ)[a]

	top adsorbed									
		$\eta_1\mu_1$(H)		$\eta_1\mu_1$(O)		di-σ adsorbed ($\eta_2\mu_2$)				
exptl[b]	θ	$^1/_3$	$^1/_4$	$^1/_6$	$^1/_9$	θ	$^1/_3$	$^1/_4$	$^1/_6$	$^1/_9$
	ν_aCH_3 (a′)	3075	3092	3082	3100	ν_aCH_3	3085	3064	3066	3071
2984[c]	ν_aCH_3 (a″)	3012	3020	3026	3004	ν_aCH_3	3042	3021	3022	3027
2984	ν_sCH_3 (a′)	2953	2964	2968	2935	ν_sCH_3	2943	2944	2947	2951
	νCH_{ald} (a′)			2777	2822	νCH	2806	2840	2838	2839
		2578	**2431**							
1667	νCO (a′)	1715	1708	**1682**	**1635**					
	δ_aCH_3 (a″)	1418	1412	1414	1424	δ_aCH_3	1459	1428	1421	1425
1430	δ_aCH_3 (a′)	1412	1404	1410	**1394**	δ_aCH_3	1409	1421	1418	1413
1365	δCCH, δ_sCH_3 (a′)	1348	1333	**1357**	**1347**	δ_sCH_3, νCC, δCCH	1359	1342	1340	1328
	δ_sCH_3, δCCH (a′)	**1325**	**1312**	**1319**	**1317**	δCCH, νCC, δ_sCH_3	**1294**	**1296**	**1295**	**1295**
1130[c]						νCO	1169	1162	1165	1172
1130	ρ_sCH_3, νCC (a′)	**1107**	**1102**	**1100**	**1096**					
	γCH, ρ_aCH_3 (a″)	1087	1077	1084	1086	νCC	1079	1071	1072	1073
						ρ_sCH_3, νPtC	**1048**	**1006**	**1000**	**980**
913	νCC, ρ_sCH_3 (a′)	**887**	**869**	**884**	**882**	γCH, ρCH_3	914	887	**884**	867
786	γCH, ρ_aCH_3 (a″)	770	758	762	779	νCO, γCH, ρCH_3	**827**	**815**	**807**	**793**
607						νPtO, δCCO, νPtC	**546**	**543**	**540**	**534**
550[c]	νPtO (PtH), δCCO (a′)	**509**	**480**	**503**	**509**					
550						νPtC, νPtO, ρCH_3	**427**	**432**	**430**	**423**

[a] Only the frequencies higher than 400 cm^{-1} are given. The values in bold correspond to the highest intensities reported in Figure 3. [b] From ref 4. [c] Some experimental frequencies are given twice, because they can be attributed to different modes depending on the geometry.

of the H-bounded geometry $\eta_1\mu_1$(H) obtained in the calculations at $^1/_3$ and $^1/_4$ ML. The experimental peak at 1667 cm^{-1} corresponds to the peaks at 1635 and 1682 cm^{-1} calculated for the $\eta_1\mu_1$(O) geometry at $^1/_9$ or $^1/_6$ ML, respectively, and is the sign of the presence of this form (Figure 3c and e). The rather large peak observed between 1365 and 1430 cm^{-1} does not appear as a single calculated peak but as multiplets between 1317 and 1394 cm^{-1} and between 1319 and 1357 cm^{-1}, at both coverages, respectively, in the same figures. The experimental peaks at 913 and 1130 cm^{-1} are found at 882 and 1096 cm^{-1} or 884 and 1100 cm^{-1} in the same calculated spectra. At this point of the comparison, the experimental spectrum fits well to that of the $\eta_1\mu_1$(O) geometry, either for a coverage of $^1/_6$ ML or for a coverage of $^1/_9$ ML. Going toward lower frequencies, a very large band, not well resolved, is observed between 400 and 800 cm^{-1}. Nevertheless, a high peak can be distinguished at 550 cm^{-1} and shoulders at 786 and 607 cm^{-1}. The first shoulder can be attributed to the peak at 807 and 793 cm^{-1} in the calculated spectra of the $\eta_2\mu_2$ geometry at coverages of $^1/_6$ and $^1/_9$ ML, respectively (Figure 3d and f). The high experimental peak at 550 cm^{-1} can be attributed as well to $\eta_1\mu_1$(O) as to $\eta_2\mu_2$ (calculated values 503−509 and 430−423, respectively). However, the calculated spectra for the $\eta_2\mu_2$ geometry, at $^1/_9$, $^1/_6$, and $^1/_3$ ML, are characterized by two peaks around 430 and 540 cm^{-1} instead of only one around 500 cm^{-1}, as is the case for $\eta_1\mu_1$(O). This is due to a supplementary interaction with the metal (Pt−C bond) and a coupling between νPtO and νPtC. The shoulder at 607 cm^{-1} in the experimental spectrum corresponds to this calculated stretch at 540−534 cm^{-1}. One notices that the calculated positions of the νPtO and νPtC stretches for both geometries deviate from the experimental values, which could be due to the lack of anharmonicity correction. The experimental peak at 607 cm^{-1} seems to be characteristic of the $\eta_2\mu_2$ geometry, since it is observed in the experimental spectra of acetaldehyde $\eta_2\mu_2$ adsorbed on Ru(001) and Rh(111).[4] Finally, there is also a small shoulder around 1000 cm^{-1} in the experimental spectrum that can correspond to the calculated frequencies at 1000 or 980 cm^{-1} in the $\eta_2\mu_2$ spectra (Figure 3d and f).

In conclusion, the main peaks and shoulders of the experimental spectrum have been attributed to $\eta_1\mu_1$(O) (1667, 1365−1430, 1130, 913, and 550 cm^{-1}) and to $\eta_2\mu_2$ (1000, 786, 607, and 550 cm^{-1}). The foregoing is an indication that acetaldehyde is adsorbed on Pt(111) as a mixture of $\eta_1\mu_1$(O) (majority) and $\eta_2\mu_2$ (minority) geometries, in agreement with their close adsorption energies (Table 2).

The vibrational frequencies calculated in the case of the alloys for the atop-Sn geometry are given in Table 6, and the spectra are reproduced in Figure 5 together with that on Pt(111) for a similar coverage. The coverage for Pt_3Sn ($^1/_8$ ML) is lower than $^1/_6$ ML, but the mean interactions between the molecules are probably similar to Pt_2Sn ($^1/_6$ ML), as is shown by identical Sn−O distances, 2.67 Å for Pt_3Sn at $^1/_8$ ML and 2.69 Å for Pt_2Sn at $^1/_6$ ML. This can be explained by the periodicity of our system (4 × 2) for Pt_3Sn ($^1/_8$ ML) in which the distance between two molecules is particularly small in one direction (see Figure 1). Therefore, we compare in Figure 5 the spectra corresponding to Pt(111) and Pt_2Sn(111) at $^1/_6$ ML and Pt_3Sn at $^1/_8$ ML. One notices a similarity between the three spectra even if some intensities are somewhat different. Globally, the peaks are more intense in the case of Pt_2Sn, as they are in the experimental spectrum, particularly the peak at 485 cm^{-1}. The main peaks are at 1691−1714 and 514−485 cm^{-1} for Pt_3Sn and Pt_2Sn, respectively (Figure 5b and c). They correspond to νCO and (νSnO, δCCO). Relative to the $\eta_1\mu_1$(O) geometry on platinum (Figure 5a), the νCO stretch is at a higher energy (1691 and 1714 vs 1682 cm^{-1}). The other peaks are at similar energies: 884−885, 1108−1095, and between 1323−1322 and 1387−1386 cm^{-1}, and they correspond to the same vibration modes. This similarity is in agreement with the experimental spectra (Figure 4), where all main peaks lie at the same energies except the νCO stretch which is shifted from 1667 to 1692 and 1713 cm^{-1} when going from Pt to Pt_3Sn and Pt_2Sn. The shift of νCO can be explained by a shorter C═O bond on the alloys (1.229 vs 1.234 Å) and mainly by a longer metal−O distance (2.67 and 2.68 vs 2.50 Å), which brings the geometry closer to the gas phase geometry, particularly in the case of Pt_2Sn. Another difference between the experimental spectra of

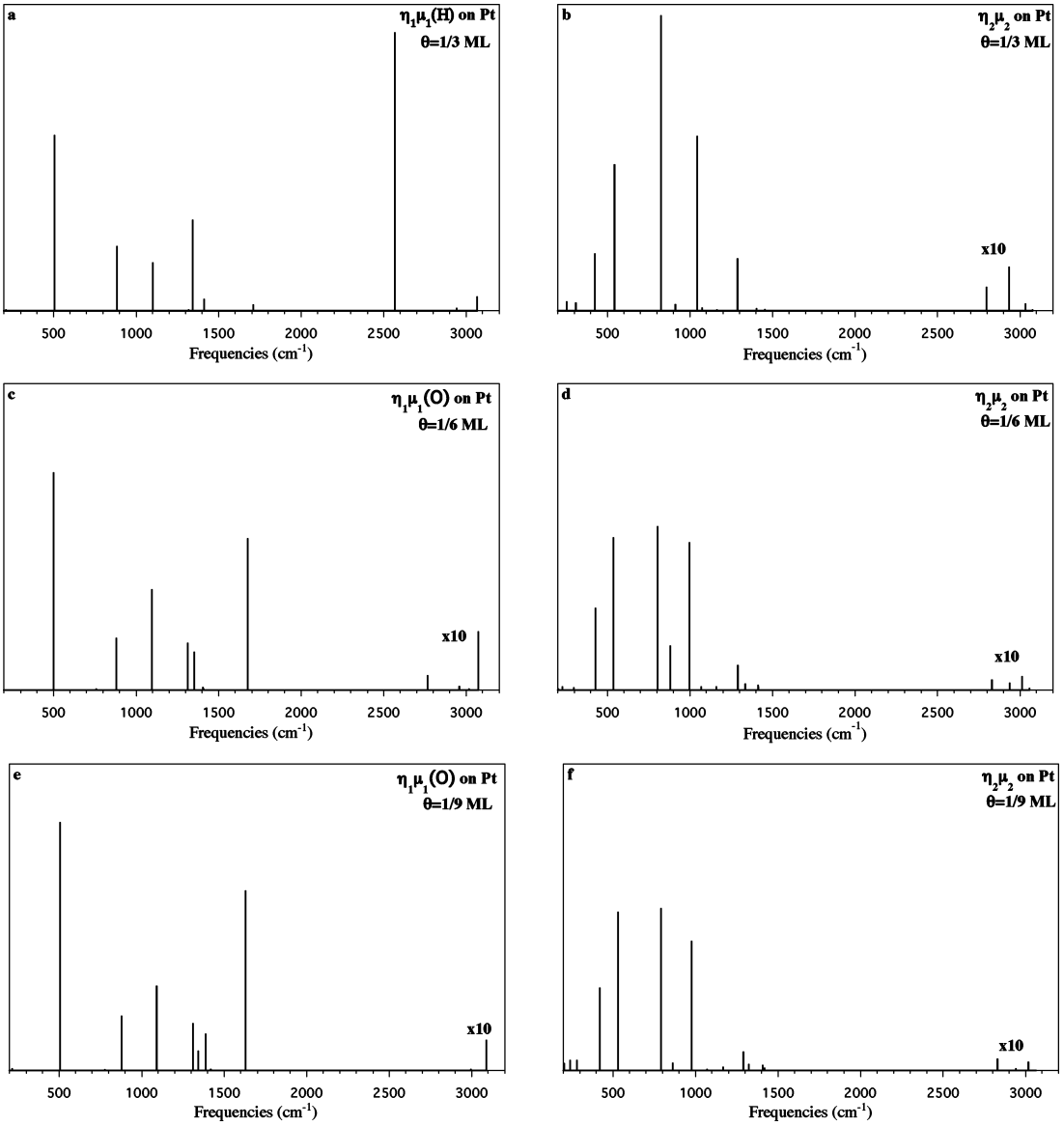

Figure 3. Calculated vibrational spectra of acetaldehyde adsorbed on Pt(111) at various coverages: (a) $\eta_1\mu_1$(H) at $^1/_3$ ML; (b) $\eta_2\mu_2$ at $^1/_3$ ML; (c) $\eta_1\mu_1$(O) at $^1/_6$ ML; (d) $\eta_2\mu_2$ at $^1/_6$ ML; (e) $\eta_1\mu_1$(O) at $^1/_9$ ML; (f) $\eta_2\mu_2$ at $^1/_9$ ML.

the alloys and that of platinum is that the νSn−O stretch appears as a sharp peak at 539 or 531 cm^{-1} and not as a broad band like on Pt. We have just explained this large band by the coexistence of the $\eta_2\mu_2$ geometry with the $\eta_1\mu_1$ one. That would mean that, on the alloys, the $\eta_2\mu_2$ geometry does not exist and only the νSnO stretch of the $\eta_1\mu_1$ form is present in the spectrum. This result is confirmed by the very small calculated adsorption energies of the $\eta_2\mu_2$ geometry on the alloys (Table 2). Hence, for the alloys, the experimental spectra correspond to only $\eta_1\mu_1$(O). From Table 6, it is evident that the spectra are similar for Pt_2Sn whatever the coverage except for the νCO stretch that is higher in the case of a coverage of $^1/_6$ ML, which better agrees with the experimental value.

The νCO shift toward higher frequencies for the alloys compared to platinum is not associated with a weaker interaction with the alloy surface, since both experimental (TPD) and theoretical results show that acetaldehyde is equally or slightly more strongly adsorbed. This is due to the fact that on the alloys the interaction with tin is partly electrostatic and does not perturb strongly the orbitals, which leads to a ν_{CO} vibration closer to the gas phase (vide infra).

DOS Analysis. We have previously studied the electronic structure of these two alloys.[9] We have found that there is an electron transfer from Sn to Pt, which results in surface Pt atoms more negatively charged in the case of the alloys and in positive charged Sn atoms. The Pt d-band gains the major part of the transferred electrons and the top of the band is farther downward from the Fermi level, as illustrated in Figure 6a and b for the d_{z2}-band. The work function changes from 5.73 eV for Pt to 5.05 and 4.86 eV for the alloys. The values are different from those published previously[9] because of the correction of the dipole effects. The occupied d-band center is 2.39, 2.55, and 2.57 eV below the Fermi level for Pt, Pt_3Sn, and Pt_2Sn, respectively. If the values of the work functions are taken into account, the occupied d-band centers are in fact at −8.12, −7.60, and −7.43 eV relative to the vacuum level for the three surfaces, respectively. Therefore, the occupied d-band center is higher in the case of the alloys than in the case of Pt.

The increase of the charge of the platinum atoms on the alloy surface explains why the electronegative oxygen atom binds less easily and is rather repelled (larger Pauli repulsion). This is a four-electron destabilizing interaction between the oxygen lone pair and the Pt d-band (essentially d_{z2}). The result is that

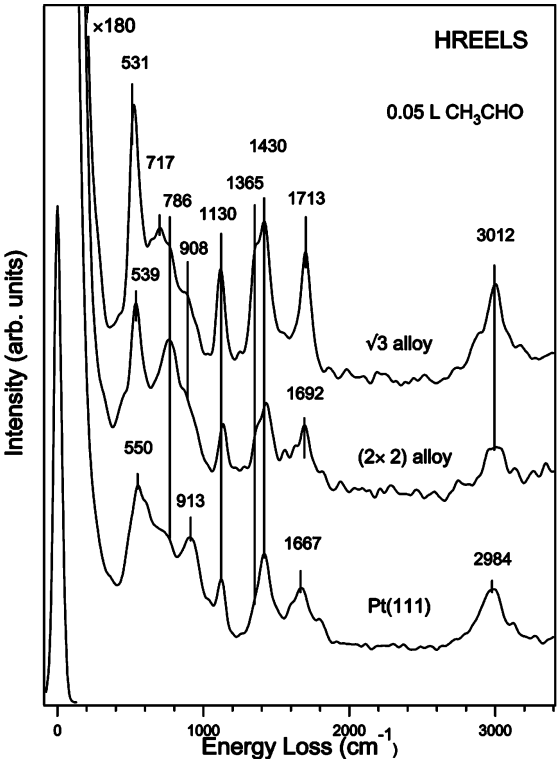

Figure 4. Experimental spectrum taken from ref 4 with the authorization of the author.

TABLE 6: Vibrational Frequencies (in cm^{-1}) of the Atop-Sn Adsorption Geometry of Acetaldehyde on $Pt_3Sn(111)$ and $Pt_2Sn(111)$[a]

	Pt_3Sn		Pt_2Sn		
	calcd $\theta = 1/8$	exptl[b]	calcd $\theta = 1/6$	calcd $\theta = 1/9$	exptl[b]
$\nu_a CH_3$ (a′)	3084	3012	3037	3093	3012
$\nu_a CH_3$ (a″)	3025		3017	3024	
$\nu_s CH_3$ (a′)	2969		2941	2971	
νCH_{ald} (a′)	2776		2815	2812	
νCO (a′)	**1691**	1692	**1714**	1692	1713
$\delta_a CH_3$ (a″)	1415	1433	1411	1418	1430
$\delta_a CH_3$ (a′)	1408		1386	1391	
δCCH (a′)	**1387**	**1365**	**1382**	1381	1365
δCH_3, δCCH (a′)	**1323**		**1322**	1321	
νCC, $\rho_s CH_3$ (a′)	**1108**	1133	**1095**	1098	1130
γCH_{ald}, $\rho_a CH_3$ (a″)	1088		1082	1095	
νCC, $\rho_s CH_3$ (a′)	**885**	908	**884**	885	908
γCH_{ald}, ρCH_3 (a″)	762	786	768	774	717
νSnO, δCCO (a′)	**514**	539	**485**	484	531

[a] Only the frequencies higher than 400 cm^{-1} are given. The values in bold correspond to the highest intensities reported in Figure 5. [b] From ref 4.

the atop geometry above a Pt atom is not stable on the alloys. On the contrary, with the sp-band of Sn being partially vacant, the interaction with the oxygen lone pair is favorable, which can lead to a non-negligible atop interaction. The variation of the work function upon adsorption has been evaluated for a coverage of $^1/_9$ ML. This is a good indication of the interaction between a molecule and a surface.[25,26] For the atop geometry, the work function decreases by 1.9 eV on Pt and 1.6 eV on the alloy Pt_2Sn, which indicates that the adsorption is effectively governed by an electron transfer from the molecule to the surface (mainly from the oxygen lone pair). For the di-σ geometry, the work function decreases by only 0.6 eV on Pt and 0.1 eV on Pt_2Sn. This shows that for this geometry also the adsorption is dominated by the donation (from π_{CO}) but partly balanced by the back-donation to π^*_{CO}.

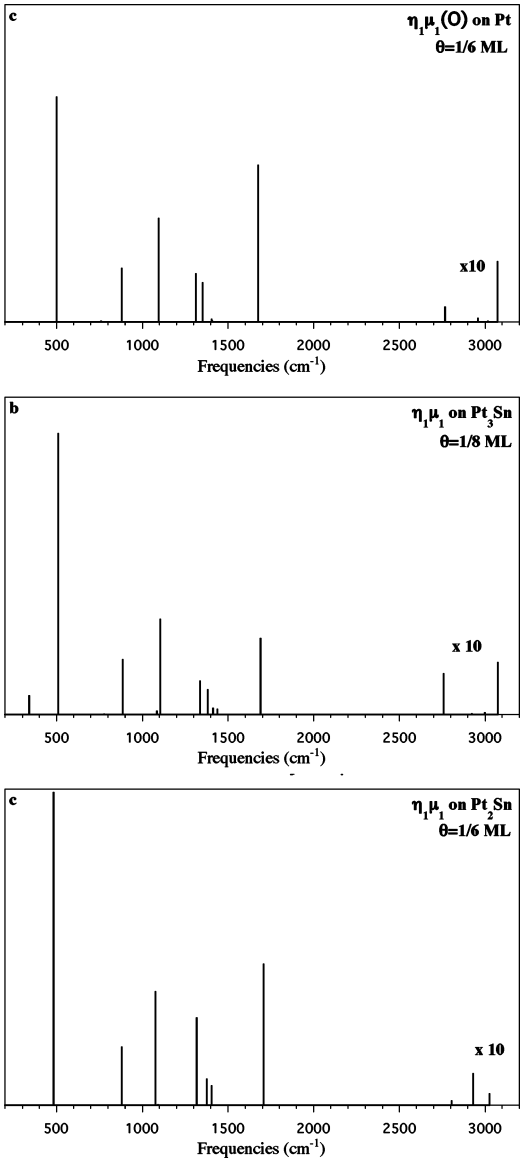

Figure 5. Calculated vibrational spectra of acetaldehyde adsorbed in the $\eta_1\mu_1$ geometry on (a) Pt ($\theta = 1/6$ ML), (b) Pt_3Sn ($\theta = 1/8$ ML), and (c) Pt_2Sn ($\theta = 1/6$ ML).

The consideration of the density of states (DOS) curves can help us to understand why the $\eta_2\mu_2$ geometry is not stable on the alloys. The orbitals that participate in a di-σ adsorption are the d_{z2} and d_{xz} metal orbitals and the π_{CO} and the π^*_{CO} orbitals of the adsorbate, as shown in Scheme 2. The DOS projected on the π system of free acetaldehyde is drawn in Figure 7. It is obtained by putting the molecule in its gas phase geometry sufficiently far from the surface to avoid any interaction and by projecting the DOS on the p_zO orbital. Four orbitals are observed: π_{CO} at -9 eV and π^*_{CO} at -2 eV mixing with π_{CH_3} at -11 eV and $\pi^*_{CH_3}$ between 1 and 5 eV. When the molecule is adsorbed, the π orbitals are enlarged and go toward lower energies and the π^*_{CO} orbital appears as a large band between the Fermi level and around -1 eV (Figure 6e and f). These changes are the sign of the interactions with the metal orbitals. In the DOS of these orbitals, the interactions are also visible: if the DOS projected on the d_{z2} orbital of an interacting platinum atom and of a noninteracting platinum atom are compared, both on Pt(111) (Figure 6c and a) and on $Pt_2Sn(111)$ (Figure 6d and b), one observes the appearance of new peaks below the Fermi level around -12.5, -9.8 and -12, -9.5 eV, respectively,

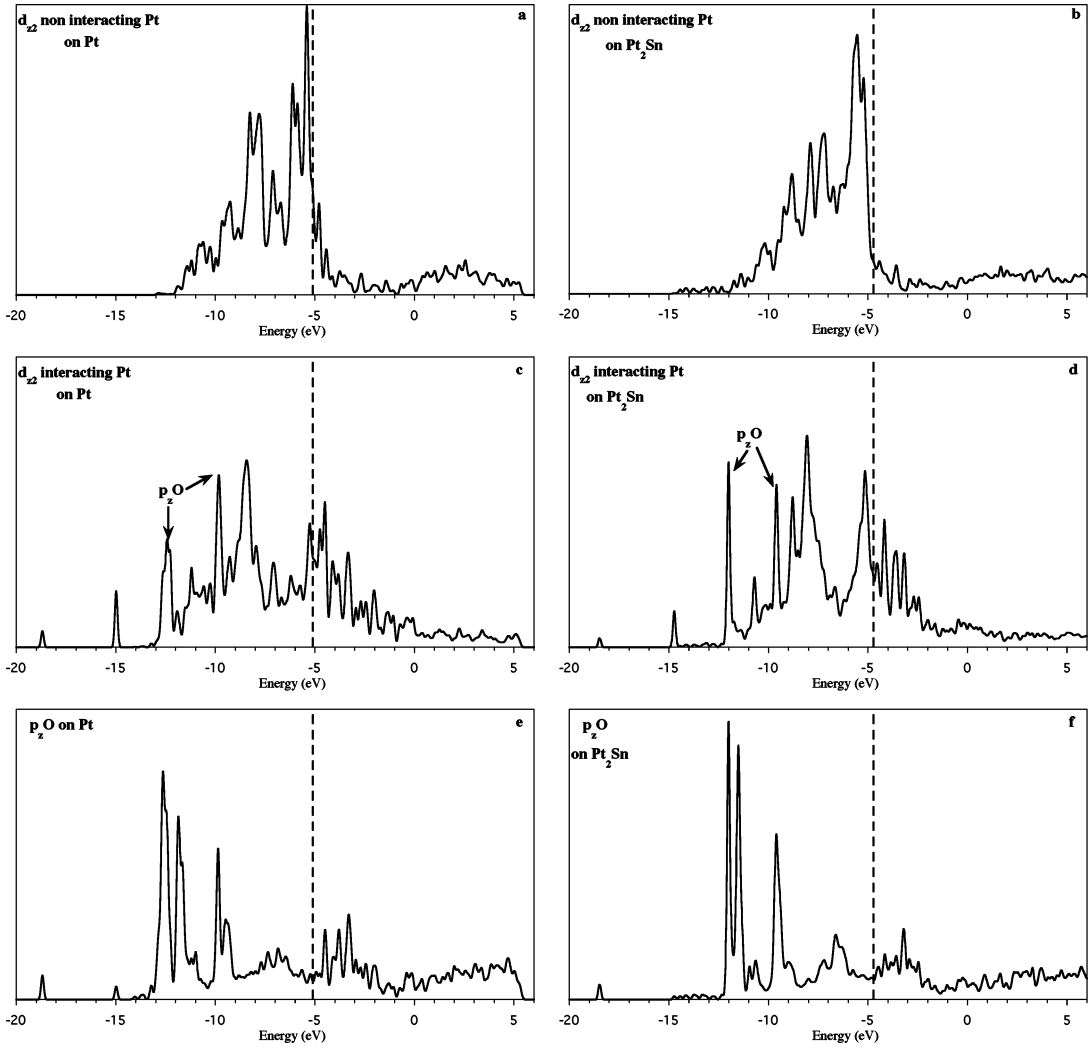

Figure 6. $\eta_2\mu_2$ adsorption mode of acetaldehyde on Pt(111) and $(\sqrt{3} \times \sqrt{3})R30°$ $Pt_2Sn(111)$: DOS projected on (a and b) the d_{z2} and d_{xz} orbitals of a noninteracting surface Pt atom, (c and d) the d_{z2} and d_{xz} orbitals of an interacting surface Pt atom, and (e and f) the p_z orbital of the oxygen atom. The dashed line indicates the Fermi level.

SCHEME 2: Schematic Interactions between the Orbitals of the Surface Atoms and the π System of Acetaldehyde in the $\eta_2\mu_2$ Geometry

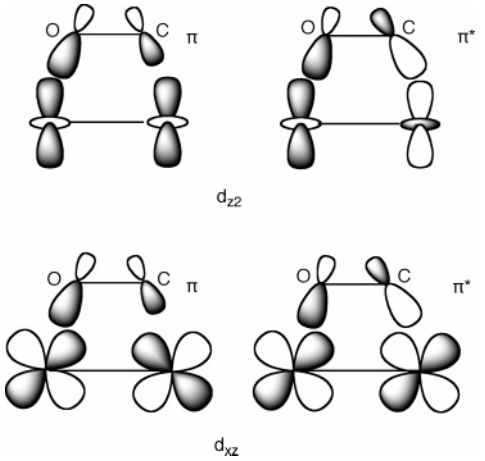

corresponding to p_zO. The π orbitals are more enlarged and go lower in energy in the case of Pt(111) than in the case of $Pt_2Sn(111)$ (Figure 6e and f). That means that their interactions with the surface are stronger for Pt(111).

After adsorption, the d_{z2} orbital is pushed away from the Fermi level E_F toward lower energies and has also a large

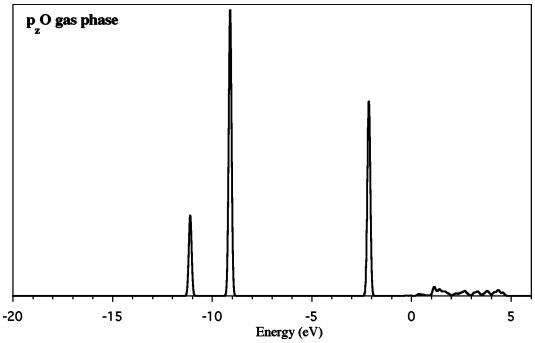

Figure 7. Acetaldehyde in the gas phase: DOS projected on p_zO.

contribution above this level. There are two possible reasons. The first one is the four-electron interactions of the Pauli type between the occupied π orbitals and the almost full d-band of platinum, which stabilize the π orbitals and destabilize the d-band. The peaks around -12.5 eV are the in-phase combination of this interaction. The crossing of part of the d-band above E_F results in a stabilizing interaction. The fact that d_{z2} is close to E_F in the case of Pt allows a large part of the band to be easily pushed above E_F after the interaction. The crossing over the Fermi level is less easy in the case of Pt_2Sn, since d_{z2} is farther from it. The second reason is the interaction of the d-band with the π^*_{CO} orbital of acetaldehyde (back-donation). Hence,

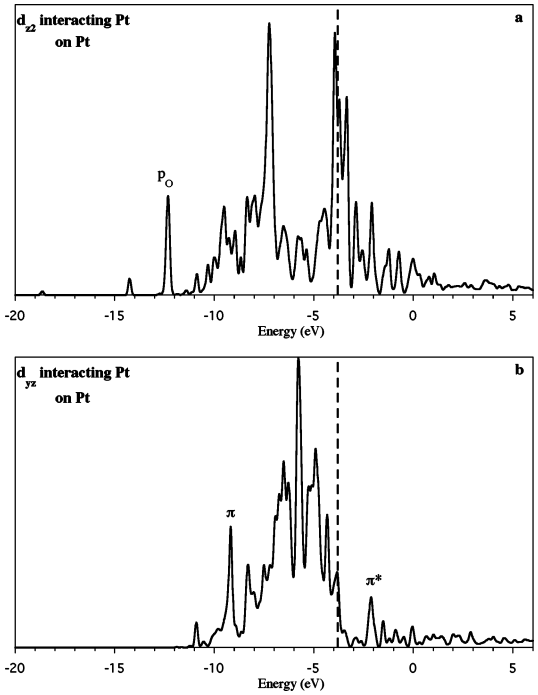

Figure 8. $\eta_1\mu_1$(O) adsorption mode of acetaldehyde on Pt(111): DOS projected on the d_{z2} and d_{yz} orbitals of an interacting surface Pt atom after adsorption.

SCHEME 3: Schematic Interactions between the Orbitals of the Surface Atoms and of Acetaldehyde in the $\eta_1\mu_1$(O) Geometry

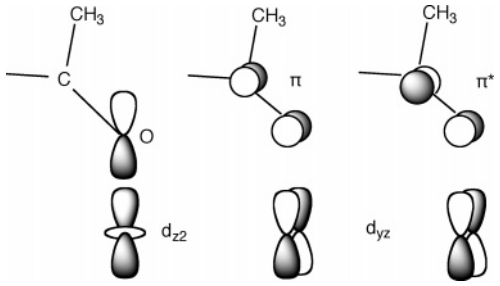

the large band between E_F and -1 eV corresponds to interactions of d_{z2} with both π_{CO} and π^*_{CO}. This is a kind of three-orbital interaction. The fraction of the d-band lying above E_F depends on the relative strength of these two interactions. It is clear from Figure 6 that the part of the d-band pushed above E_F is more important in the case of Pt(111), which is the sign of a better interaction than in the case of the alloys. The downward movement of the d-band center is also larger for Pt (0.32 eV) than for Pt_2Sn (0.12 eV).

Regarding the atop adsorption, the DOS projected on the d_{z2} and d_{yz} orbitals of the interacting Pt atom are plotted in Figure 8 in the case of Pt(111). In the former, one observes a peak at -12.3 eV corresponding to the lone pair of the oxygen atom, following Scheme 3. Moreover, on the DOS projected on d_{yz}, two peaks at -9.2 and -2.1 eV are present, corresponding to π_{CO} and π^*_{CO}, respectively. That means that the π system also plays a role in the atop adsorption. In the case of Pt_2Sn, the interactions occur essentially between p_zO and the s orbital of the Sn atom and are rather weak. The interaction with p_zSn exists but is small. This results in a long Sn$-$O bond (Table 1). To explain the value of the adsorption energy, electrostatic interactions must also be invoked, since the Sn atoms are positively charged.

This is a general trend that the unsaturated molecules interacting with the surface by a π system with donation and back-donation are less strongly adsorbed on the alloys Pt/Sn than on Pt. This has been observed experimentally for alkenes[27] and CO[28] and theoretically for acrolein[9] and cyclopentene.[29] This is also obtained in the present work for the di-σ adsorption and for the atop adsorption on a Pt atom. However, the adsorption energy is found to be stronger or equal on the alloys when the adsorption of acetaldehyde takes place at an electron deficient Sn atom. The same result has been observed for other aldehydes.[9]

Conclusion

The DFT calculations presented here compared the adsorption geometries of acetaldehyde on Pt(111) and on two PtSn alloys. On Pt, the energy values showed that acetaldehyde can adsorb both $\eta_1\mu_1$ and $\eta_2\mu_2$ at low or medium coverage. At high coverage, the $\eta_2\mu_2$ form is less competitive and acetaldehyde prefers a geometry where the adsorption takes place through the aldehydic hydrogen and no longer through the oxygen, as far as the molecules are periodically distributed on the surface. The calculated vibrational spectra allowed us to conclude that the experimental spectrum on Pt(111) corresponds to a mixture of $\eta_1\mu_1$ (majority) and $\eta_2\mu_2$ (minority) species. On the Pd/Sn alloys, only the $\eta_1\mu_1$ geometry exists, where the oxygen atom is bound to a Sn atom (atop-Sn). In contrast to the situation observed with η_2-bound molecules, the adsorption energies are equal to that on Pt(111) in agreement with the TPD experiments. This shows that the often observed decrease of the adsorption energy on Pt/Sn compared to Pt is not a general rule but depends on the interaction type. Moreover, the shift of the νCO stretch toward higher energies is not correlated with a decrease of the adsorption energy, owing to the partial electrostatic character of the interaction. The calculated DOS curves allowed us to understand the relative stability of the species on Pt/Sn and Pt.

The presence of $\eta_2\mu_2$ adsorbed acetaldehyde on Pt(111) could explain the decomposition into acetyl that is experimentally observed.[4] Indeed, this reaction is exothermic and the barrier has been calculated to be 20 kJ/mol.[30] In contrast, the absence of the $\eta_2\mu_2$ form on the Pt/Sn alloys could be the reason no decomposition occurs on these surfaces.

Acknowledgment. The authors acknowledge D. Loffreda for fruitful discussions. They thank the Institut du Développement et des Ressources en Informatique Scientifique (IDRIS) at Orsay (project 609) and the Centre Informatique National de l'Enseignement Supérieur (CINES) at Montpellier for CPU time.

References and Notes

(1) Marinelli, T. B. L. W.; Nabuurs, S.; Ponec, V. *J. Catal.* **1995**, *151*, 431.
(2) McCabe, R. W.; Di Maggio, C. L.; Madix, R. J. *J. Phys. Chem.* **1985**, *89*, 854.
(3) Rodriguez, J. L.; Pastor, E.; Xia, X. H.; Iwasita, T. *Langmuir* **2000**, *16*, 5479.
(4) Zhao, H.; Kim, J.; Koel, B. E. *Surf. Sci.* **2003**, *538*, 147.
(5) Gursahani, K. I.; Alcalá, R.; Cortright, R. D.; Dumesic, J. A. *Appl. Catal., A* **2001**, *222*, 369.
(6) Alcalá, R.; Mavrikakis, M.; Dumesic, J. A. *J. Catal.* **2003**, *218*, 178.
(7) Alcalá, R.; Greeley, J.; Mavrikakis, M.; Dumesic, J. A. *J. Chem. Phys.* **2002**, *116*, 8973.
(8) Delbecq, F.; Sautet, P. *J. Catal.* **2002**, *211*, 398.
(9) Delbecq, F.; Sautet, P. *J. Catal.* **2003**, *220*, 115.
(10) Kresse, G.; Hafner, J. *Phys. Rev. B* **1993**, *47*, 558.
(11) Kresse, G.; Hafner, J. *Phys. Rev. B* **1993**, *48*, 13115.
(12) Kresse, G.; Hafner, J. *Phys. Rev. B* **1994**, *49*, 14251.
(13) Perdew, J. P.; Wang, Y. *Phys. Rev. B* **1992**, *45*, 13244.

(14) Kresse, G.; Hafner, J. *Phys. Rev. B* **1998**, *59*, 1758.
(15) Atrei, A.; Bardi, U.; Wu, J. X.; Zanazzi, E.; Rovida, G. *Surf. Sci.* **1993**, *290*, 286.
(16) Galeotti, M.; Atrei, A.; Bardi, U.; Rovida, G.; Torrini, M. *Surf. Sci.* **1994**, *313*, 349.
(17) Loffreda, D.; Jugnet, Y.; Delbecq, F.; Bertolini, J. C.; Sautet, P. *J. Phys. Chem. B* **2004**, *108*, 9085.
(18) Morikawa, Y. *Phys. Rev. B* **2001**, *63*, 033405.
(19) Loffreda, D.; Delbecq, F.; Vigné, F.; Sautet, P. Manuscript to be published.
(20) Hollenstein, H.; Günthard, H. H. *Spectrochim. Acta, Part A* **1971**, *27*, 2027.
(21) Hollenstein, H. *Mol. Phys.* **1980**, *39*, 1013.
(22) Hollenstein, H.; Winther, F. *J. Mol. Spectrosc.* **1978**, *71*, 118.
(23) Raval, R.; Chesters, M. A. *Surf. Sci. Lett.* **1989**, *219*, L505.
(24) Hostetler, M. J.; Nuzzo, R. G.; Girolami, G. S.; Dubois, L. H. *Organometallics* **1995**, *14*, 3377.
(25) Leung, T. C.; Kaa, C. C.; Su, W. S.; Feng, Y. J.; Chang, C. T. *Phys. Rev. B* **2003**, *68*, 195408.
(26) Nieuwenhuys, B. E. *Surf. Sci.* **1981**, *105*, 505.
(27) Tsai, Y.-L.; Xu, C.; Koel, B. E. *Surf. Sci*. **1997**, *385*, 37.
(28) Paffett, M. T.; Gebhard, S. C.; Windham, R. G.; Koel, B. E. *J. Phys. Chem.* **1990**, *94*, 6831.
(29) Becker, C.; Delbecq, F.; Breitbach, J.; Hamm, G.; Franke, D.; Wandelt, K. *J. Phys. Chem. B* **2004**, *108*, 18960.
(30) Gursahani, K. I.; Alcalá, R.; Cortright, R. D.; Dumesic, J. A. *Appl. Catal., A* **2001**, *222*, 369.